We are IntechOpen, the world's leading publisher of Open Access books Built by scientists, for scientists

4,800
Open access books available

122,000
International authors and editors

135M
Downloads

Our authors are among the

154
Countries delivered to

TOP 1%
most cited scientists

12.2%
Contributors from top 500 universities

CLARIVATE ANALYTICS BOOK CITATION INDEX INDEXED

WEB OF SCIENCE™

Selection of our books indexed in the Book Citation Index in Web of Science™ Core Collection (BKCI)

Interested in publishing with us?
Contact book.department@intechopen.com

Numbers displayed above are based on latest data collected.
For more information visit www.intechopen.com

13

DC/DC Converters for Electric Vehicles

Monzer Al Sakka[1], Joeri Van Mierlo[1] and Hamid Gualous[2]
[1]*Vrije Universiteit Brussel,*
[2]*Université de Caen Basse-Normandie*
[1]*Belgium,*
[2]*France*

1. Introduction

The large number of automobiles in use around the world has caused and continues to cause serious problems of environment and human life. Air pollution, global warming, and the rapid depletion of the earth's petroleum resources are now serious problems. Electric Vehicles (EVs), Hybrid Electric Vehicles (HEVs) and Fuel Cell Electric Vehicles (FCEVs) have been typically proposed to replace conventional vehicles in the near future. Most electric and hybrid electric configurations use two energy storage devices, one with high energy storage capability, called the "main energy system" (MES), and the other with high power capability and reversibility, called the "rechargeable energy storage system" (RESS). MES provides extended driving range, and RESS provides good acceleration and regenerative braking. Energy storage or supply devices vary their output voltage with load or state of charge and the high voltage of the DC-link create major challenges for vehicle designers when integrating energy storage / supply devices with a traction drive. DC-DC converters can be used to interface the elements in the electric power train by boosting or chopping the voltage levels. Due to the automotive constraints, the power converter structure has to be reliable, lightweight, small volume, with high efficiency, low electromagnetic interference and low current/voltage ripple. Thus, in this chapter, a comparative study on three DC/DC converters topologies (Conventional step-up dc-dc converter, interleaved 4-channels step-up dc-dc converter with independent inductors and Full-Bridge step-up dc-dc converter) is carried out. The modeling and the control of each topology are presented. Simulations of 30KW DC/DC converter are carried out for each topology. This study takes into account the weight, volume, current and voltage ripples, Electromagnetic Interference (EMI) and the efficiency of each converter topology.

2. Electric vehicles powertrain

An Electric Vehicle is a vehicle that uses a combination of different energy sources, Fuel Cells (FCs), Batteries and Supercapacitors (SCs) to power an electric drive system as shown in Fig. 1. In EV the main energy source is assisted by one or more energy storage devices. Thereby the system cost, mass, and volume can be decreased, and a significant better performance can be obtained. Two often used energy storage devices are batteries and SC_S. They can be connected to the fuel cell stack in many ways. A simple configuration is to

directly connect two devices in parallel, (FC/battery, FC/SC, or battery/SC). However, in this way the power drawn from each device cannot be controlled, but is passively determined by the impedance of the devices. The impedance depends on many parameters, e.g. temperature, state-of-charge, health, and point of operation. Each device might therefore be operated at an inappropriate condition, e.g. health and efficiency. The voltage characteristics also have to match perfectly of the two devices, and only a fraction of the range of operation of the devices can be utilized, e.g. in a fuel cell battery configuration the fuel cell must provide almost the same power all the time due to the fixed voltage of the battery, and in a battery/supercapacitor configuration only a fraction of the energy exchange capability of the supercapacitor can be used. This is again due to the nearly constant voltage of the battery. By introducing DC/DC converters one can chose the voltage variation of the devices and the power of each device can be controlled (Schaltz & Rasmussen, 2008).

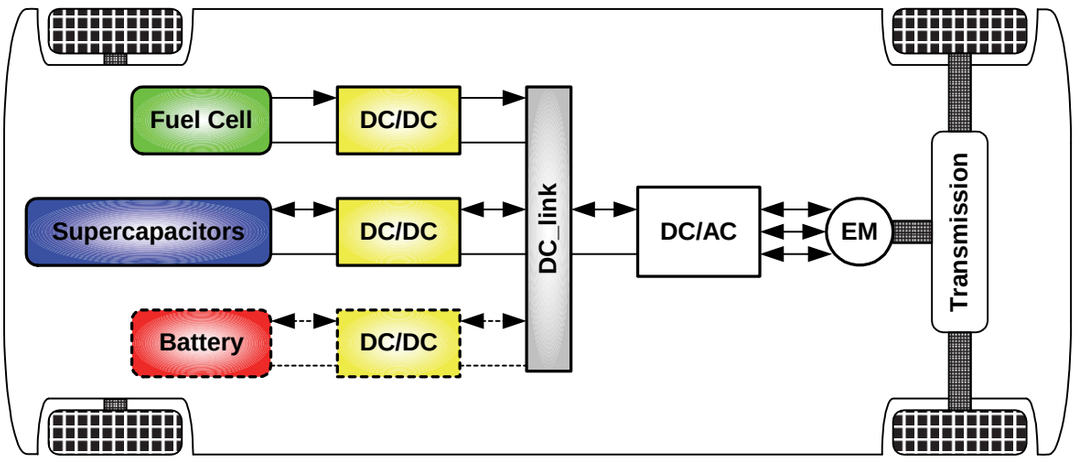

Fig. 1. Electric vehicle drive system.

In reference (Schaltz & Rasmussen, 2008), 10 cases of combining the fuel cell with the battery, SCs, or both are investigated. The system volume, mass, efficiency, and battery lifetime were compared. It is concluded that when SCs are the only energy storage device the system becomes too big and heavy. A fuel cell/battery/supercapacitors hybrid provides the longest life time of the batteries. It can be noticed that the use of high power DC/DC converters is necessary for EV power supply system. The power of the DC/DC converter depends on the characteristics of the vehicle such as top speed, acceleration time from 0 to 100 Km/h, weight, maximum torque, and power profile (peak power, continuous power) (Büchi et al., 2006). Generally, for passenger cars, the power of the converter is more than 20 KW and it can go up to 100 KW.

3. DC/DC converters for electric vehicles

The different configurations of EV power supply show that at least one DC/DC converter is necessary to interface the FC, the Battery or the Supercapacitors module to the DC-link.
In electric engineering, a DC to DC converter is a category of power converters and it is an electric circuit which converts a source of direct current (DC) from one voltage level to another, by storing the input energy temporarily and then releasing that energy to the

output at a different voltage. The storage may be in either magnetic field storage components (inductors, transformers) or electric field storage components (capacitors).
DC/DC converters can be designed to transfer power in only one direction, from the input to the output. However, almost all DC/DC converter topologies can be made bi-directional. A bi-directional converter can move power in either direction, which is useful in applications requiring regenerative braking.
The amount of power flow between the input and the output can be controlled by adjusting the duty cycle (ratio of on/off time of the switch). Usually, this is done to control the output voltage, the input current, the output current, or to maintain a constant power. Transformer-based converters may provide isolation between the input and the output. The main drawbacks of switching converters include complexity, electronic noise and high cost for some topologies. Many different types of DC/DC power converters are proposed in literature (Chiu & Lin, 2006), (Fengyan et al., 2006). The most common DC/DC converters can be grouped as follows:

3.1 Non-isolated converters

The non-isolated converters type is generally used where the voltage needs to be stepped up or down by a relatively small ratio (less than 4:1). And when there is no problem with the output and input having no dielectric isolation. There are five main types of converter in this non-isolated group, usually called the buck, boost, buck-boost, Cuk and charge-pump converters. The buck converter is used for voltage step-down, while the boost converter is used for voltage step-up. The buck-boost and Cuk converters can be used for either step-down or step-up. The charge-pump converter is used for either voltage step-up or voltage inversion, but only in relatively low power applications.

3.2 Isolated converters

Usually, in this type of converters a high frequency transformer is used. In the applications where the output needs to be completely isolated from the input, an isolated converter is necessary. There are many types of converters in this group such as Half-Bridge, Full-Bridge, Fly-back, Forward and Push-Pull DC/DC converters (Garcia et al., 2005), (Cacciato et al., 2004). All of these converters can be used as bi-directional converters and the ratio of stepping down or stepping up the voltage is high.

3.3 Electric vehicle converters requirements

In case of interfacing the Fuel Cell, the DC/DC converter is used to boost the Fuel Cell voltage and to regulate the DC-link voltage. However, a reversible DC/DC converter is needed to interface the SCs module. A wide variety of DC-DC converters topologies, including structures with direct energy conversion, structures with intermediate storage components (with or without transformer coupling), have been published (Lachichi & Schofield, 2006), (Yu & Lai, 2008), (Bouhalli et al., 2008). However some design considerations are essential for automotive applications:

- Light weight,
- High efficiency,
- Small volume,
- Low electromagnetic interference,
- Low current ripple drawn from the Fuel Cell or the battery,
- The step up function of the converter,

- Control of the DC/DC converter power flow subject to the wide voltage variation on the converter input.

Each converter topology has its advantages and its drawbacks. For example, The DC/DC boost converter does not meet the criteria of electrical isolation. Moreover, the large variance in magnitude between the input and output imposes severe stresses on the switch and this topology suffers from high current and voltage ripples and also big volume and weight. A basic interleaved multichannel DC/DC converter topology permits to reduce the input and output current and voltage ripples, to reduce the volume and weight of the inductors and to increase the efficiency. These structures, however, can not work efficiently when a high voltage step-up ratio is required since the duty cycle is limited by circuit impedance leading to a maximum step-up ratio of approximately 4. Hence, two series connected step-up converters would be required to achieve the specific voltage gain of the application specification. A full-bridge DC/DC converter is the most frequently implemented circuit configuration for fuel-cell power conditioning when electrical isolation is required. The full bridge DC/DC converter is suitable for high-power transmission because switch voltage and current are not high. It has small input and output current and voltage ripples. The full-bridge topology is a favorite for zero voltage switching (ZVS) pulse width modulation (PWM) techniques.

4. Electromagnetic compatibility regulation

Fast semiconductor devices make it possible to have high speed and high frequency switching in power electronics converters. High speed switching helps to reduce weight and volume of equipment; however, it causes some undesirable effects such as radio frequency interference (RFI) emission. It is believed that high dv/dt or di/dt due to modern power device switching is mainly responsible for the EMI emissions. Application of electrical equipment especially static power electronic converters in different equipment is increasing more and more. Power electronics converters are considered as an important source of electromagnetic interference and have undesirable effects on the electric networks. Some residential, commercial and especially medical consumers are very sensitive to power system disturbances including voltage and frequency variations. Also, for Electric vehicle, there is limitation of the EMI. The best solution to reduce the interference and improve the power quality is complying national or international EMC regulations. CISPR, IEC, FCC and VDE are among the best known organizations from Europe, USA and Germany who are responsible for determining and publishing the most important EMC regulations. Compliance of regulations is evaluated by comparison of measured or calculated conducted interference level in the mentioned frequency range with the stated requirements in regulations. In European community compliance of regulation is mandatory and products must have certified label to show covering of requirements (Farhadi & Jalilian, 2006). For Electric Vehicle, the maximum interference level should meet the DIN VDE 0879 standard. The limits in this standard are almost the same as the class B of VDE 0871 requirement and limitation on conducted emission.

4.1 Electromagnetic conducted interference measurement

A Line Impedance Stabilization Network (LISN) is typically designed to allow for measurements of the electromagnetic interference existing on the power line, it is a device

used to create known impedance on power lines of electrical equipment during electromagnetic interference testing. The stated situation is shown in Fig. 2.

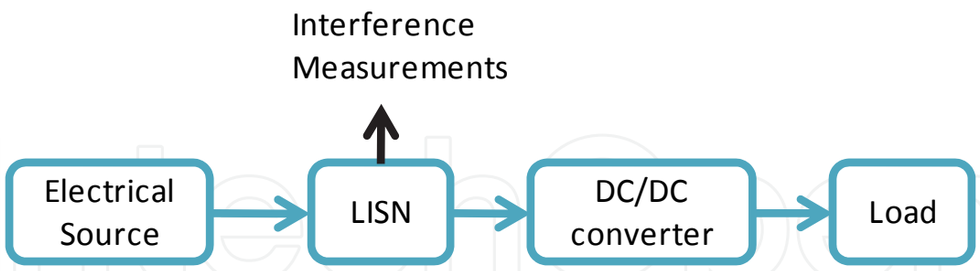

Fig. 2. LISN placement to measure conducted interference.

Variation of level of signal at the output of LISN versus frequency is the spectrum of interference. The electromagnetic compatibility of a device can be evaluated by comparison of its interference spectrum with the standard limitations. The level of signal at the output of LISN in frequency range 10 kHz up to 30 MHz or 150 kHz up to 30 MHz is criteria of compatibility and should be under the standard limitations. Converting the results to dBuV (Equation 1) makes it possible to compare the spectrum of interference with standard requirements. In practical situations, the LISN output is connected to a spectrum analyzer and interference measurement is carried out. But for modeling and simulation purposes, the LISN output spectrum must be calculated using appropriate software.

$$dB\mu V(x) = 20\log_{10}\left(\frac{x}{10^{-6}}\right) = 20\log_{10}(x) + 120 \tag{1}$$

5. Losses in a power converter

The considered losses in a power converter are the losses produced by the semiconductors switches (IGBTs and DIODES) and the passive components (capacitors and inductors). The aim of this explanation is only to give an idea about the losses estimation. This estimation is used in this study to calculate the efficiency. The efficiency of a power converter is given by:

$$\eta = \frac{P_{Input\_power} - \sum Losses}{P_{Input\_power}} \tag{2}$$

5.1 IGBT conduction and switching losses

The IGBT conduction losses are given by:

$$P_{IGBT\_cond} = V_{CE0}\langle I_{IGBT}\rangle + r_{CE}I^2_{IGBT\_rms} \tag{3}$$

The IGBT characteristics (V_{CE0} and r_{CE}) are given in the datasheet of the IGBT. $\langle I_{IGBT}\rangle$ and I_{IGBT_rms} are the average current and the rms current of the IGBT, respectively.
The IGBT switching losses are given by:

$$P_{IGBT\_switch} = \left(E_{on} + E_{off}\right)f_s \tag{4}$$

Where, f_s is the switching frequency. E_{on} and E_{off} are the switching losses during the switching on and switching off, respectively.
Energy values are generally given for specific test conditions (Voltage test condition V_{CC}). Thus, to adapt these values to others test conditions, as an estimation the IGBT switching losses are given by (Garcia Arregui, 2007):

$$P_{IGBT\_switch} = \frac{V_{IGBT}}{V_{CC}}\left(E_{on}\left(I_{IGBT\_on}\right) + E_{off}\left(I_{IGBT\_off}\right)\right) f_s \tag{5}$$

5.2 Diode conduction and switching losses

The Diode conduction losses are given by:

$$P_{D\_cond} = V_{F0}\langle I_D \rangle + r_F I_{D\_rms}^2 \tag{6}$$

The Diode characteristics (V_{F0} and r_F) are given in the Diode datasheet. $<I_D>$ and I_{D_rms} are the average current and the rms current of the Diode, respectively.
The Diode switching losses are given by:

$$P_{D\_switch} = E_{rr} f_s \tag{7}$$

Where, f_s is the switching frequency. E_{rr} is the recovery energy.
The recovery energy is given as a function of the voltage, the current, the turn-on and turn off resistances and for a specific test conditions. To adapt the previous expression to another test conditions, as estimation the diode switching losses are given by:

$$P_{D\_switch} = \frac{V_D}{V_{CC}} E_{rr}\left(I_D\right) f_s \tag{8}$$

5.3 Capacitor losses

The capacitor losses are calculated thanks to the equivalent resistance of the capacitor, which is usually given in the datasheets. The capacitor losses are given by:

$$P_{Capacitor} = r_C I_{C\_rms}^2 \tag{9}$$

Where, r_C is the equivalent resistance of the capacitor and I_{C_rms} is the rms current value of the capacitor.

5.4 Inductors losses

In an inductor, there are iron and copper losses. Core losses (or iron losses) are energy losses that occur in electrical transformers and inductors using magnetic cores. The losses are due to a variety of mechanisms related to the fluctuating magnetic field, such as eddy currents and hysteretic phenomena. Most of the energy is released as heat, although some may appear as noise. These losses are estimated based on charts supplied by magnetic core manufacturer. To estimate the total iron losses, the weight of core should be multiplied by the obtained value for a specific flux density and switching frequency. The inductor iron losses are given by:

$$P_{L\_Core} = W_{core} P_{core} \tag{10}$$

Where, W_{core} is the weight of the core and P_{core} is the iron losses per Kg.
The copper losses or the conduction losses in the inductor are given by:

$$P_{L\_copper} = r_L I_{L\_rms}^2 \tag{11}$$

Where, rL is the resistance of the inductor and I_{L_rms} is the rms current value of the inductor.

6. Design, modeling, control and simulation results of 3 DC/DC converters

The modeling of studied converters is done by using the Simpower tools of Matlab/Simulink, and it takes into account the IGBT and Diodes parameters (real components) and the inductors and capacitors losses. To achieve accurate voltage regulation, two control loops are used as shown in Fig. 3. This control mode (current mode control) requires knowledge of the inductor current, which is controlled via the inner loop. The outer loop manages the output voltage error by commanding the necessary current. The control was done using RST controllers.

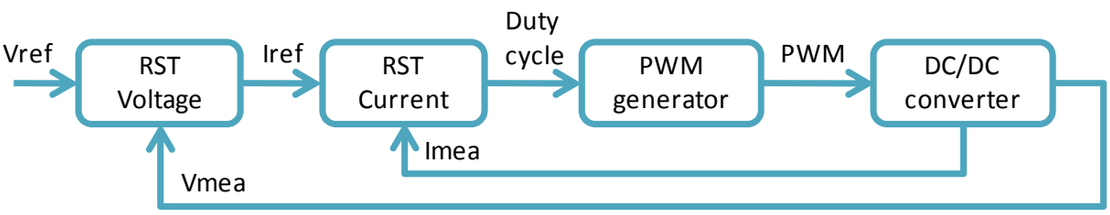

Fig. 3. Block diagram of control mode.

6.1 RST controller

The canonical structure of the RST controller is presented in Fig. 4. This structure has two degrees of freedom, i.e., the digital filters R and S are designed in order to achieve the desired regulation performance, and the digital filter T is designed afterwards in order to achieve the desired tracking and regulation. This structure allows achievement of different levels of performance in tracking and regulation. The case of a controller operating on the regulation error (which does not allow the independent specification of tracking and regulation performance) corresponds to T=R. Digital PID controller can also be represented in this form, leading to particular choices of R, S and T (Landau, 1998).

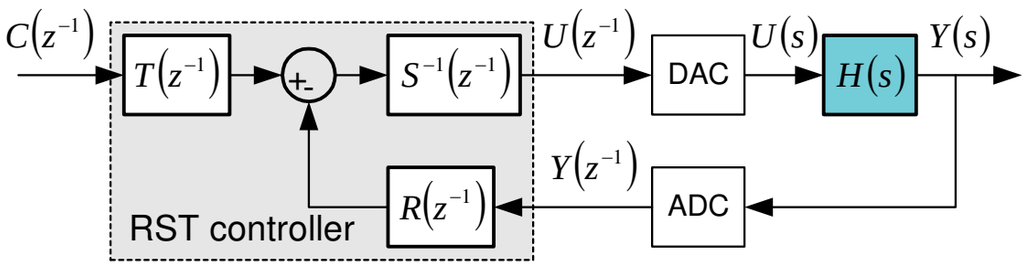

Fig. 4. The RST canonical structure of a digital controller

The equation of the RST canonical controller is give by:

$$S\left(z^{-1}\right)\cdot U\left(z^{-1}\right)+R\left(z^{-1}\right)\cdot Y\left(z^{-1}\right)=T\left(z^{-1}\right)\cdot C\left(z^{-1}\right) \tag{12}$$

Where:

- $U(z^{-1})$: the input of the plant H(s),
- $Y(z^{-1})$: the output of the plant H(s),
- $C(z^{-1})$: the desired tracking trajectory.

The polynomials $R(z^{-1})$, $S(z^{-1})$ and $T(z^{-1})$ have the following form:

$$\begin{cases} R\left(z^{-1}\right)=r_0+r_1z^{-1}+...+r_{n_R}z^{-n_R} \\ S\left(z^{-1}\right)=s_0+s_1z^{-1}+...+s_{n_S}z^{-n_S} \\ T\left(z^{-1}\right)=t_0+t_1z^{-1}+...+t_{n_T}z^{-n_T} \end{cases} \tag{13}$$

The plant and closed-loop models are expressed by expression 14 and expression 15 respectively:

$$H(s)=\frac{Y(s)}{U(s)}=\frac{B(s)}{A(s)} \tag{14}$$

$$H_{CL}(s)=\frac{Y(s)}{C(s)}=\frac{B_{CL}(s)}{A_{CL}(s)} \tag{15}$$

A formal discretization leads to both discrete-time transfer functions as follows, with m<=n and d is a pure time delay.

$$H\left(z^{-1}\right)=z^{-d}\frac{B\left(z^{-1}\right)}{A\left(z^{-1}\right)}=z^{-d}\frac{b_1z^{-1}+b_2z^{-2}+...+b_mz^{-m}}{a_1z^{-1}+a_2z^{-2}+...+a_nz^{-n}} \tag{16}$$

$$H_{CL}\left(z^{-1}\right)=\frac{Y\left(z^{-1}\right)}{C\left(z^{-1}\right)}=\frac{B_{CL}\left(z^{-1}\right)}{A_{CL}\left(z^{-1}\right)} \tag{17}$$

The closed-loop transfer operator (between $C(z^{-1})$ and $Y(z^{-1})$) is given by:

$$H_{CL}\left(z^{-1}\right)=\frac{B\left(z^{-1}\right)T\left(z^{-1}\right)}{A\left(z^{-1}\right)S\left(z^{-1}\right)+B\left(z^{-1}\right)R\left(z^{-1}\right)}=\frac{B_{CL}\left(z^{-1}\right)}{A_{CL}\left(z^{-1}\right)} \tag{18}$$

R, S and T polynomials are determined in order to obtain an imposed closed-loop system. Resolving the Diophantine equation (or Bezout's identity) $AS+BR=A_{CL}$ leads to the identification of S and R polynomials. The polynomial T is determined from the equation $BT=B_{CL}$.

6.1.1 Calculation of RST parameters used in this study

The current and voltage control loops controllers of the three DC/DC topologies compared in this study use the same type of transfer function in open loop which is given by:

$$H(s)=\frac{Y(s)}{U(s)}=\frac{1}{ks} \tag{19}$$

A formal discretization leads to the discrete-time transfer function as follows:

$$\begin{aligned} H\left(z^{-1}\right) &= \left(1-z^{-1}\right)TFZ\left\{\frac{1}{s}H(s)\right\} \\ &= \left(1-z^{-1}\right)\frac{T_s}{k}\frac{z}{(z-1)^2}=\frac{T_s}{k}\frac{z^{-1}}{1-z^{-1}}=\frac{B\left(z^{-1}\right)}{A\left(z^{-1}\right)} \end{aligned} \tag{20}$$

The sampling period T_s used in the control is equal to the switching frequency of PWM signals.

Choosing the polynomials $R(z^{-1})$ and $S(z^{-1})$:

- The system in closed-loop should be a two order system ($\deg(A_{CL}(z^{-1}))=2$).
- Error Specification: no error in steady state step response and rejection of disturbance.

The polynomials $R(z^{-1})$ and $S(z^{-1})$ are given by:

$$\begin{aligned} &\deg\left(S\left(z^{-1}\right)\right)=\deg\left(R\left(z^{-1}\right)\right)=\deg\left(A_{CL}\left(z^{-1}\right)\right)-1 \\ &\Rightarrow\begin{cases} S\left(z^{-1}\right)=1-z^{-1} \\ R\left(z^{-1}\right)=r_0+r_1z^{-1} \end{cases} \end{aligned} \tag{21}$$

In addition, in order to guarantee a unity static gain in closed-loop:

$$\begin{cases} \lim\limits_{z\to 1}H_{CL}\left(z^{-1}\right)=\dfrac{B(1)\cdot T}{A(1)S(1)+B(1)R(1)}=1 \\ S(1)=0 \end{cases} \Rightarrow T=R(1)=r_0+r_1 \tag{22}$$

Calculation of $S(z^{-1})$ and $R(z^{-1})$ coefficients:

The desired closed loop polynomial is given by:

$$A_{CL}\left(z^{-1}\right)=A\left(z^{-1}\right)S\left(z^{-1}\right)+B\left(z^{-1}\right)R\left(z^{-1}\right)=1+p_1z^{-1}+p_2z^{-2} \tag{23}$$

Replacing $A(z^{-1})$, $S(z^{-1})$, $B(z^{-1})$ and $R(z^{-1})$ by their expressions in Equation 23. The obtained polynomial of the desired closed-loop is represented by:

$$\begin{aligned} A_{CL}\left(z^{-1}\right) &= 1+p_1z^{-1}+p_2z^{-2} \\ &= 1+\left(\frac{T_s}{k}r_0-2\right)z^{-1}+\left(\frac{T_s}{k}r_1-2\right)z^{-2} \end{aligned} \tag{24}$$

By identification the coefficients r_0 and r_1 are given by:

$$\begin{cases} r_0=\dfrac{k}{T_s}(p_1+2) \\ r_1=\dfrac{k}{T_s}(p_2-1) \end{cases} \tag{26}$$

The coefficients p_1 and p_2 are determined according to the desired current and voltage closed-loop dynamics.
Finally, the desired closed loop polynomial can be represented by:

$$A_{CL}\left(z^{-1}\right)=\left(1-z^{-1}e^{-\omega_n T_s}\right)^2 \tag{26}$$

Where, ω_n is the bandwidth of the control loop.

6.2 Boost DC/DC converter

A boost DC/DC converter (step-up converter shown in Fig. 5.) is a power converter with an output DC voltage greater than its input DC voltage. It is a class of switching-mode power supply containing at least two semiconductor switches (a diode and a switch) and at least one energy storage element (capacitor and/or inductor). Filters made of capacitors are normally added to the output of the converter to reduce output voltage ripple and the inductor connected in series with the input DC source in order to reduce the current ripple.

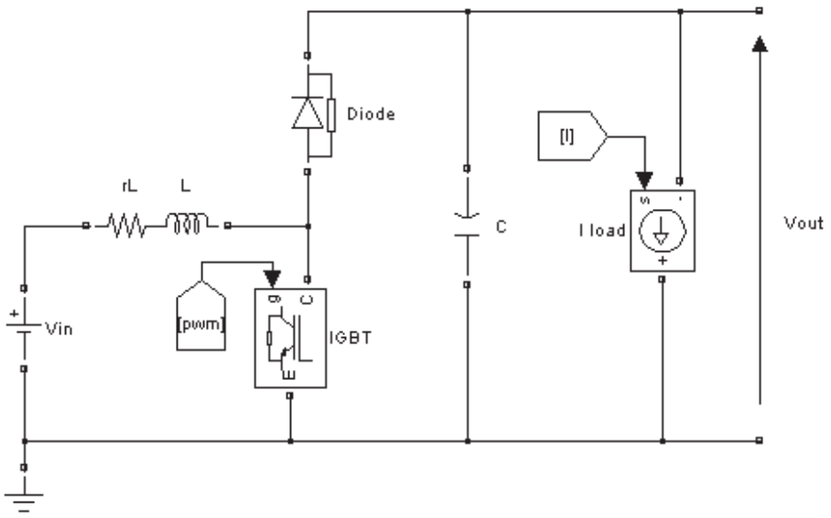

Fig. 5. Standard step-up DC-DC converter.

The smoothing inductor L is used to limit the current ripple. The filter capacitor C can restrict the output voltage ripples. The ripple current in the inductor is calculated by neglecting the output voltage ripple. The inductance value is given by the following equation:

$$L=\frac{V_{out}}{4\times F\times \Delta IL_{\max}}=400\mu H \tag{27}$$

The capacitor must be able to keep the current supply at peak power. The output voltage ripple is a result of alternative current in the capacitor.

$$C=\frac{IL_{\max}}{4\times F\times \Delta V_{out\_\max}}=781\mu F \tag{28}$$

Where:

- V_{out} : the output voltage,
- ΔIL_{max} : the inductor current ripple,
- F : the switching frequency.
- IL_{max} : the maximum input current,
- ΔV_{out_max} : the maximum output voltage ripple.

Table 1 shows the specifications of the converter. The inductor current ripple value is desired to be less than 5% of the maximum input current in the case of interfacing a Fuel Cell. A ripple factor less than 4% for the Fuel Cell's output current will have negligible impact on the conditions within the Fuel Cell diffusion layer and thus will not severely impact the Fuel Cell lifetime (Yu et al., 2007).

ΔV_{out_max}	Output voltage ripple (1% of V_{out} = 4 V)
V_{out}	Output voltage (400 V)
F	Switching frequency (20 KHz)
IL_{max}	Inductor current (250 A)
ΔILmax	Inductor current ripple (5% of ILmax = 12.5 A)

Table 1. Standard boost DC-DC converter parameters

6.2.1 Modeling and control

The output voltage is adjustable via the duty cycle α of the PWM signal switching the IGBT as given in the following expression:

$$\frac{V_{out}}{V_{in}} = \frac{1}{1-\alpha} \tag{29}$$

The input voltage Vin is considered as constant (200V). The inductor and capacitor resistances are not taken into account in the analysis of the converter. The converter can be modeled by the following system of equations:

$$\begin{cases} v_{in} = L\dfrac{di_L}{dt} + (1-u)v_{out} \\ i_L(1-u) = C\dfrac{dv_{out}}{dt} + i_{out} \end{cases} \tag{30}$$

This model can be used directly to simulate the converter. By replacing the variable u by its average value which is the duty cycle during a sampling period makes it possible to obtain the average model of the converter as illustrated in the following system of differential equations:

$$\begin{cases} v_{in} = L\dfrac{di_L}{dt} + (1-\alpha)v_{out} \\ il(1-\alpha) = C\dfrac{dv_{out}}{dt} + i_{out} \end{cases} \tag{31}$$

Current control loop

The current control loop guarantees limited variations of the current trough the inductor during important load variations. The inductor current and voltage models are given by Equation 32 and Equation 33, respectively.

$$IL(s) = \frac{1}{Ls}\left(V_{in}(s) - \left(1 - \alpha(s)\right) \cdot V_{out}(s)\right) \tag{32}$$

$$VL(s) = V_{in}(s) - \left(1 - \alpha(s)\right) \cdot V_{out}(s) \tag{33}$$

To make it simple to define a controller, the behavior of the system should be linearized. The linearization is done by using an inverse model. Thus an expression between the output of corrector and the voltage of the inductor should be found (Lachaize, 2004). Thus, the following expression is proposed:

$$\alpha(s) = 1 + \frac{VL'(s) - V_{in}(s)}{V_{out}(s)} \tag{34}$$

Where, VL' is a new control variable represents the voltage reference of the inductor.
Thus, a linear transfer between VL'(s) and IL(s) is obtained by:

$$T_1(s) = \frac{IL(s)}{VL'(s)} = \frac{1}{Ls} \tag{35}$$

The structure of the regulator is a RST form. The polynomials R, S and T are calculated using the methodology explained above. The bandwidth of the current loop ω_i should be ten times lower than the switching frequency.

$$f_i \le \frac{f}{10}, \omega_i \le \frac{2\pi f}{10} \tag{36}$$

The inductor current loop is shown in Fig. 6.

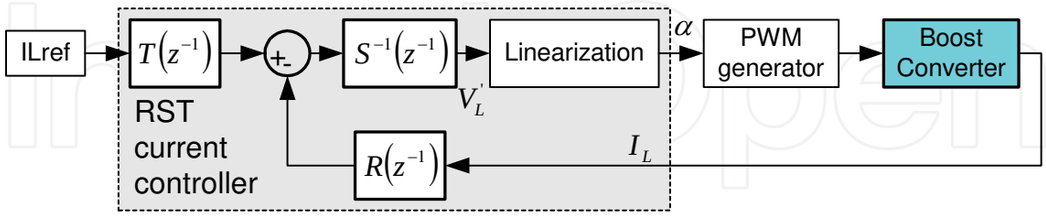

Fig. 6. Boost converter inductor current loop

From the reference value of the current and its measured value, The RST current controller block will calculate the duty cycle as explained above.

Voltage control loop

The output voltage loop was designed following a similar strategy to the current loop. To define the voltage controller, it is assumed that the current control loop is perfect. The capacitor current and voltage models are given by Equation 37 and Equation 38, respectively.

$$IC(s) = (1-\alpha(s)) \cdot IL(s) - I_{out}(s) \tag{37}$$

$$VC(s) = \frac{1}{Cs}\left((1-\alpha(s)) \cdot IL(s) - I_{out}(s)\right) \tag{38}$$

The linearization of the system is done by the following expression:

$$\begin{aligned} IL(s) &= \frac{\left(IC'(s) + I_{out}(s)\right)}{(1-\alpha(s))} \\ \Rightarrow I_{Lref}(s) &= \frac{V_{out}(s)}{V_{in}(s)}\left(IC'(s) + I_{out}(s)\right) \end{aligned} \tag{39}$$

Where IC′ is a new control variable represents the current reference of the capacitor.
Thus, a linear transfer between Vout(s) and IC′(s) is obtained by:

$$T_2(s) = \frac{V_{out}(s)}{IC'(s)} = \frac{1}{Cs} \tag{40}$$

The bandwidth of the voltage loop ω_v should be ten times lower than the current loop bandwidth ω_i which means hundred times lower than the switching frequency.

$$f_v \le \frac{f}{100}, \omega_v \le \frac{2\pi f}{100} \tag{41}$$

The output voltage control loop is shown in Fig. 7.

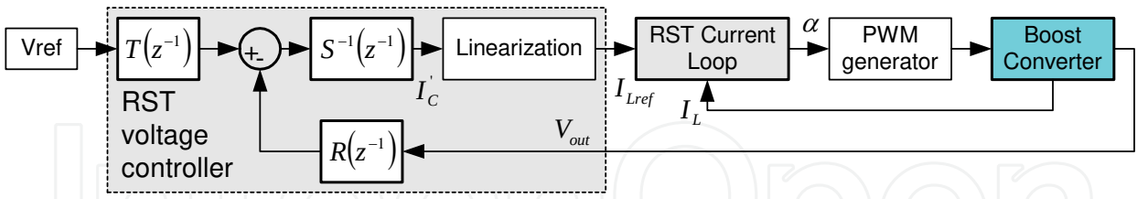

Fig. 7. Boost converter output voltage control loop.

The RST voltage controller operates in the same as the current controller and it has to calculate the current reference which will be the input of the current controller.

Simulation results

The current and voltage ripples are about 10 Amps and 2 Volts, respectively. The results show that the converter follows the demand on power thanks to the good control.
The efficiency of the boost dc/dc converter is about 83% at full load as shown in Fig. 8.
Fig. 9 shows the spectrum of the output signal of the LISN as described in the section "Electromagnetic compatibility regulation". It is seen that the level of conducted interference due to converter is not tolerable by the regulations. As a consequence EMI filter suppression is necessary to meet the terms the regulations.

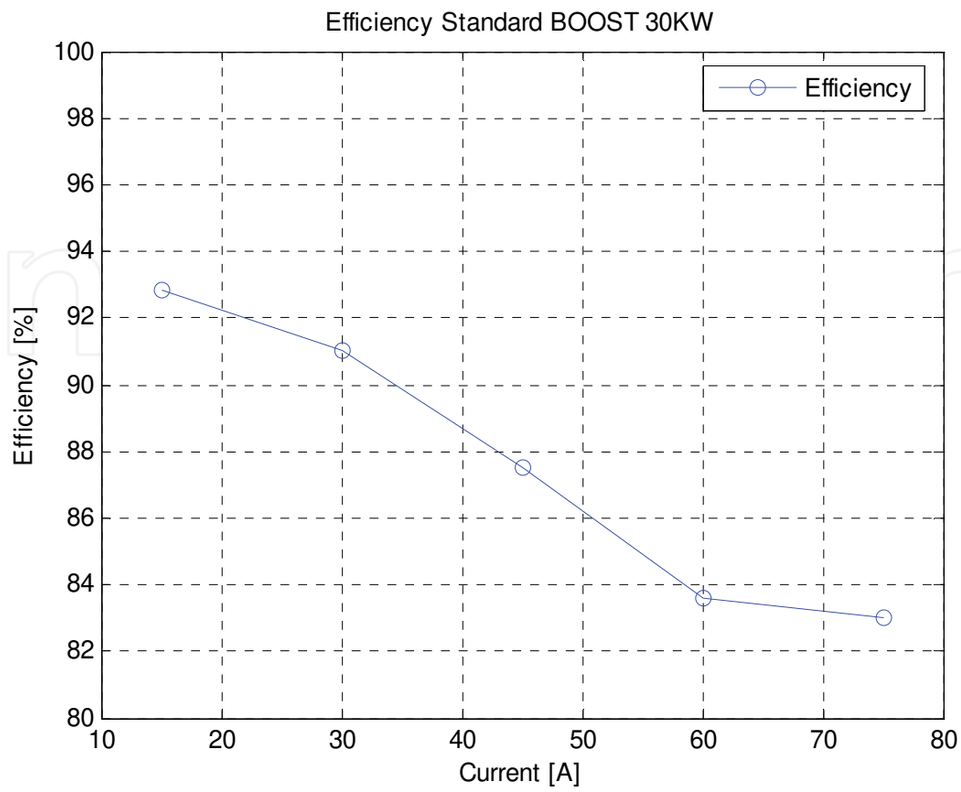

Fig. 8. Boost converter efficiency versus current load

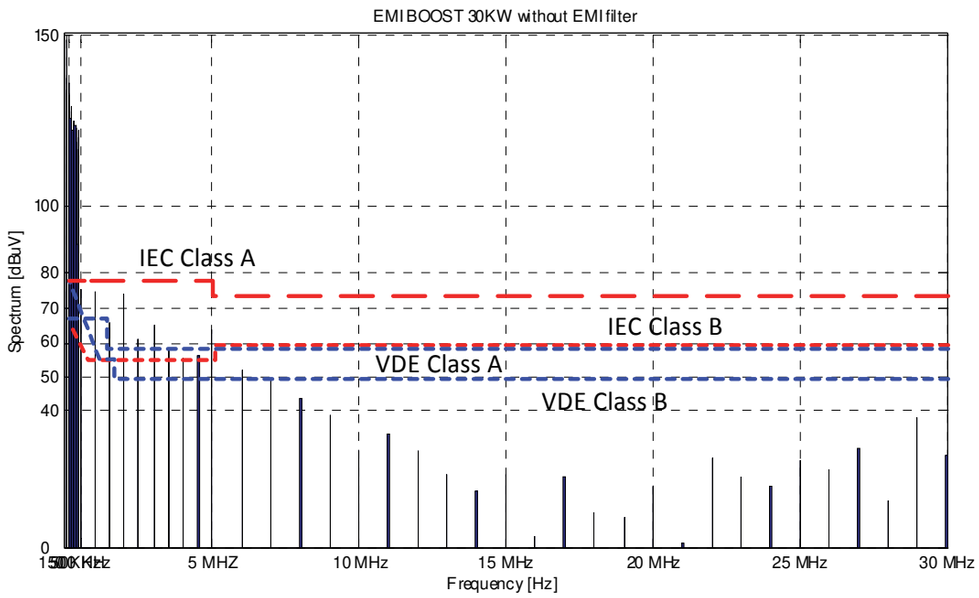

Fig. 9. EMI simulation results of boost DC/DC converter.

6.3 Interleaved 4-channel DC/DC converter

Fig. 10 shows a basic interleaved step-up converter of 4 identical levels where the inductances L1 to L4 are built by a separate magnetic core. The gate signals to the power switching devices are successively phase shifted by T/N where T is the switching period and N the number of channels. Thus, the current delivered by the electric source is shared equally between each basic step-up converter level and has a ripple content of period T/N (Destraz et al., 2006).

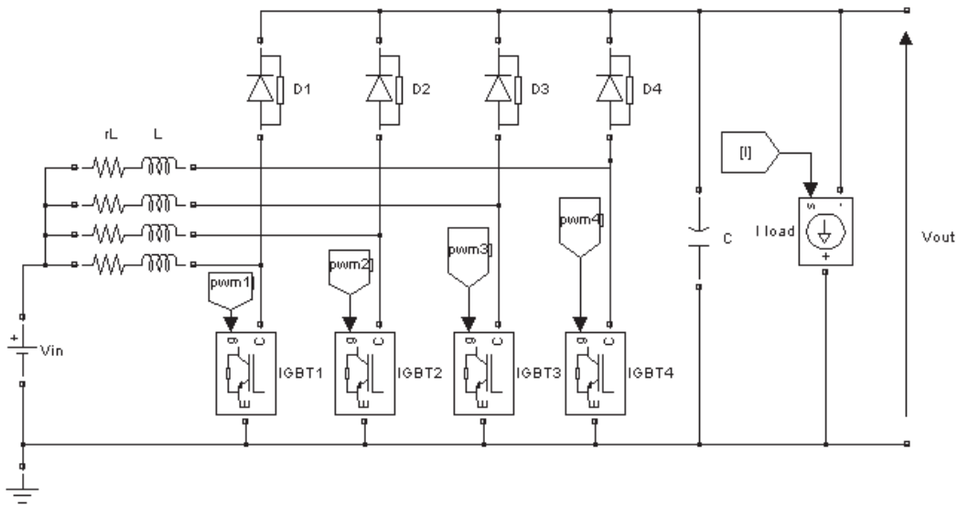

Fig. 10. Interleaved 4-channels step-up DC-DC converter.

The design of the 4-channels converter is the same like the boost one. The output voltage is adjustable via the duty cycle α of the PWM signal switching the IGBTs as given in the following expression:

$$\frac{V_{out}}{V_{in}} = \frac{1}{1-\alpha} \tag{42}$$

Where:

- α : the duty cycle,
- V_{in} : the input voltage,
- V_{out} : the output voltage.

The inductor value of each channel is given by the following expression:

$$L_k = \frac{V_{out}}{4 \times F \times N \times \Delta I_{In\_\max}} = 100\mu H \tag{43}$$

Where:

- N : the number of channels,
- ΔI_{In_max} : the input current ripple,
- F : the switching frequency.
- I_{In_max} : the maximum input current,
- ΔV_{out_max} : the maximum output voltage ripple.

As control signals are interleaved and the phase angle is 360°/N, the frequency of the total current is N times higher than the switching frequency F. The filter capacitor of the interleaved N-channel dc-dc converter is given by the following expression:

$$C_{f\min} = \frac{I_{In\_\max}}{4 \times F \times N \times \Delta V_{out\_\max}} = 195\mu F \tag{44}$$

Table 2 shows the specifications of the converter.

ΔV_{out_max}	Output voltage ripple (1% of V_{out} = 4 V)
V_{out}	Output voltage (400 V)
F	Switching frequency (20 KHz)
I_{In_max}	Inductor current (250 A)
ΔI_{In_max}	Input current ripple (5% of I_{In_max} = 12.5 A)

Table 2. Interleaved 4-channels DC-DC converter parameters

6.3.1 Modeling and control

The 4-channel converter is modeled in the same way of the boost converter. The current and voltage loop are designed also using the same methodology used for boost converter. The calculated current reference is divided by 4 (number of channels). The output voltage control loop is shown is Fig. 11.

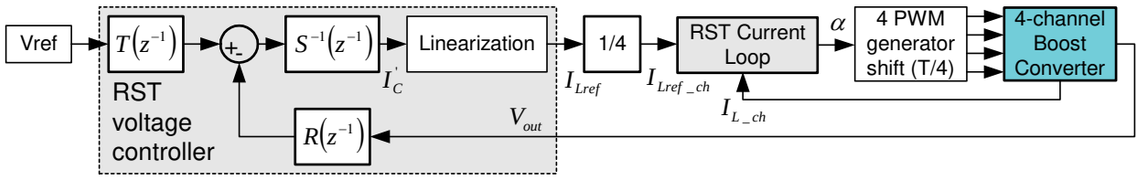

Fig. 11. 4-channels converter output voltage control loop.

In the proposed control, the duty cycle is calculated from one reference channel. The same duty cycle is applied to the other channels. The PWM signals are shifted by 360/4°.

Simulation results

Thanks to the interleaving technique, the total current ripples are reduced and can be neglected; the voltage ripples are about 0.5V. The results show that the converter follows the demand on power.

The efficiency of the 4-channels dc/dc converter is about 92% at full load as shown in Fig. 12. The drop in efficiency is due to the changing from discontinuous mode (DCM) to continuous mode (CM). In DCM, the technique of zero voltage switching (ZVS) is operating which permits to reduce the switching losses in the switch, thus the efficiency is increased.

Fig. 13 shows the EMI of the interleaved 4-channels DC/DC converter. It is seen that the level of conducted interference due to converter is not tolerable by the regulations. As a consequence this converter without EMI filter suppression does not meet the terms of the regulations. Thus, EMI filter suppression is required.

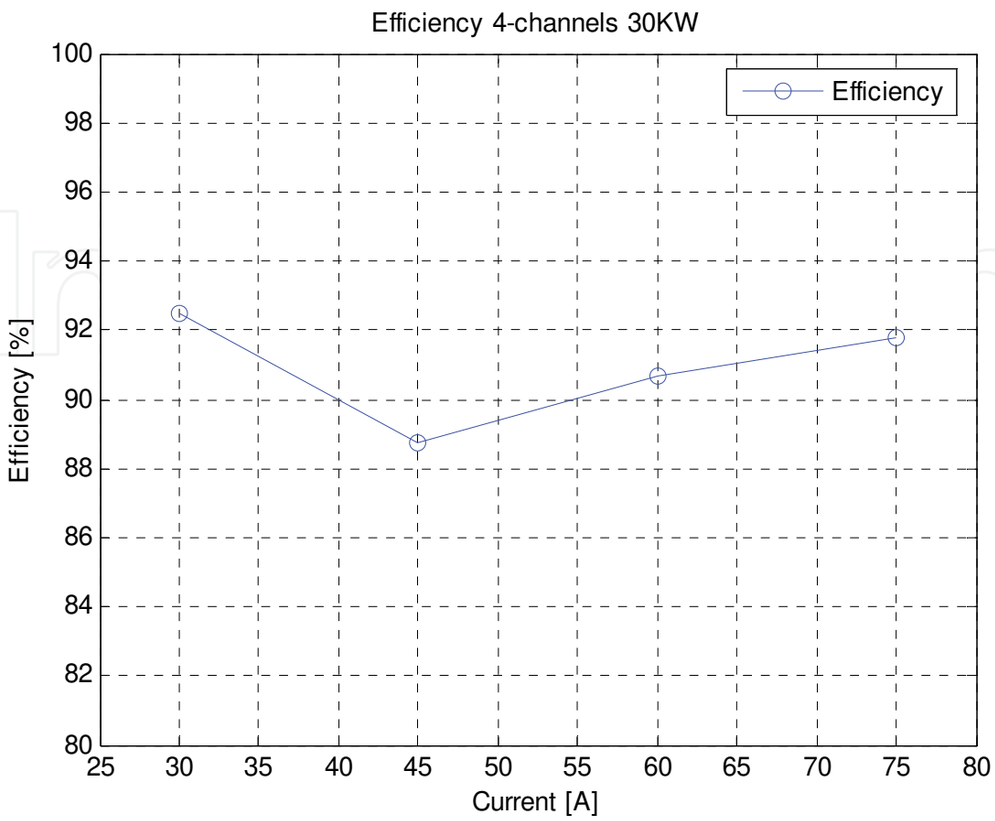

Fig. 12. 4-channels converter efficiency versus current load.

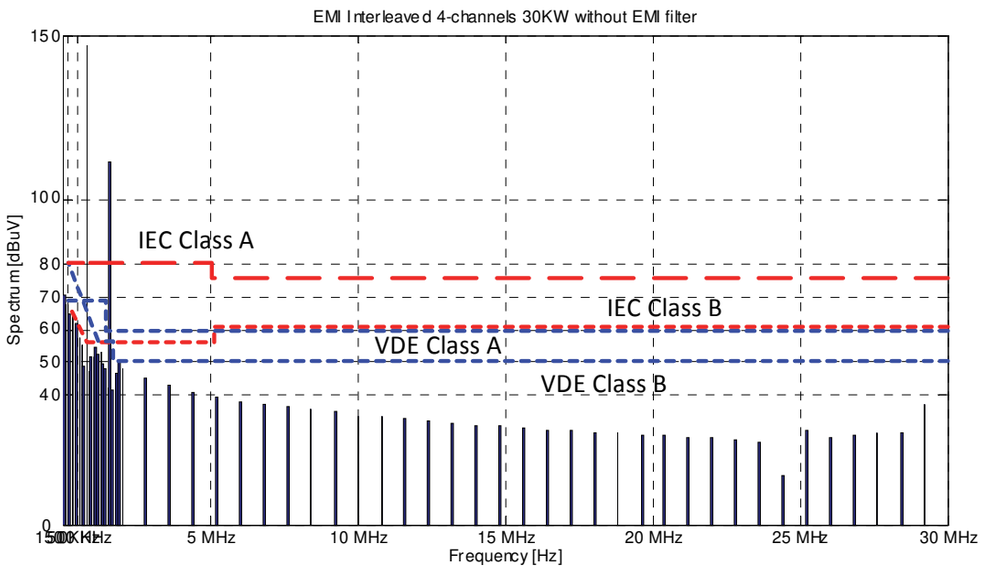

Fig. 13. EMI simulation results of interleaved 4-channels DC/DC converter.

6.4 Full-bridge DC/DC converter

The structure of this topology is given in Fig. 14. The transformer turns ratio n must be calculated in function of the minimum input voltage (Pepa, 2004).

$$n = \frac{N_s}{N_p} = \frac{1}{2\alpha} \times \frac{V_{out}}{V_{in\_\min}} \tag{45}$$

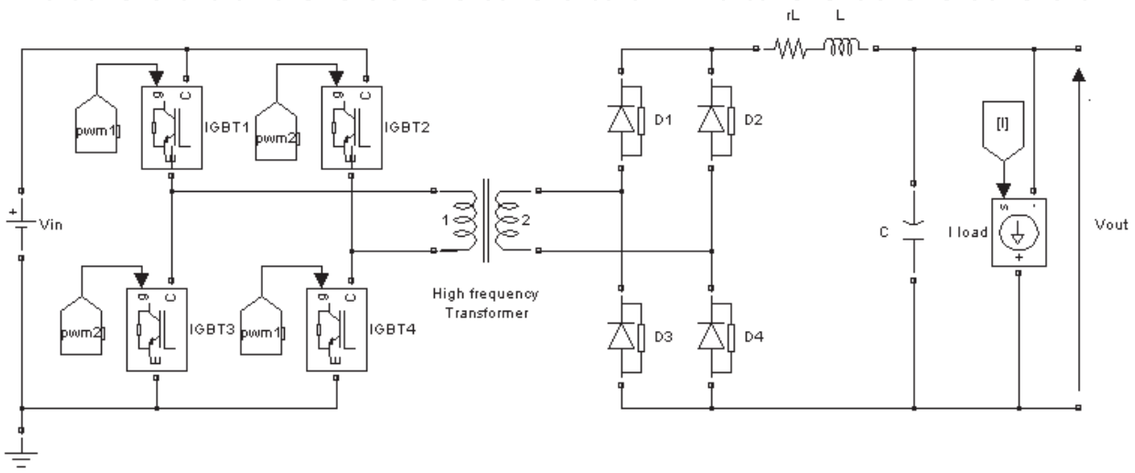

Fig. 14. Full-bridge step-up DC-DC converter

The output filter inductor and capacitor values could be calculated based on maximum ripple current and ripple voltage magnitudes. The calculations are done considering the converter is working in CCM.

$$L = \frac{n \times \alpha \times V_{in}}{2 \times \Delta IL_{\max} \times F} = 1.2\text{mH} \tag{46}$$

The filter capacitor value is given by the following relation based on the inductor current ripple value and the output voltage ripple.

$$C = \frac{\Delta IL_{\max}}{8 \times \Delta V_{out\_\max} \times F} = 14.64\mu\text{F} \tag{47}$$

Where:

- α : the duty cycle,
- N_s : the number of turns in the secondary winding of the transformer,
- N_P : the number of turns in the primary winding of the transformer,
- V_{in} : the input voltage,
- ΔIL_{max} : the inductor current ripple,
- F : the switching frequency,
- ΔV_{out_max} is the maximum output voltage ripple.

Table 3 shows the simulations parameters of the converter.

ΔV_{out_max}	Output voltage ripple (1% of V_{out} = 4 V)
V_{out}	Output voltage (400 V)
F	Switching frequency (40 KHz)
ΔIL_{max}	Inductor current ripple (5% of ILmax = 3.75 A)
n	Transformer turns ratio (= 4)

Table 3. Full-Bridge DC-DC converter parameters.

6.4.1 Modeling and control

The Full-Bridge DC/DC converter will have to maintain a constant 400V DC output. By increasing and decreasing the duty cycle α=t/T of the PWM signals, the output voltage can be held constant with a varying input voltage. The output voltage can be calculated as follows:

$$V_{out} = \frac{2}{T}\int_0^t \frac{V_{in}}{n} dt \Rightarrow V_{out} = 2 \times n \times \alpha \times V \tag{48}$$

Where, T is the switching period (T=1/F), n is the transformer turns ration (n=Ns/Np), and t is the pulse width time.

The inductor current and voltage models are obtained by expressions 49 and 50, respectively.

$$I_L(s) = \frac{1}{Ls}\left(\frac{4n\sqrt{2}}{\pi}\alpha(s) \times V_{in}(s) - V_{out}(s)\right) \tag{49}$$

$$V_L(s) = \frac{4n\sqrt{2}}{\pi}\alpha(s) \times V_{in}(s) - V_{out}(s) \tag{50}$$

The linearization of the system is done by using an inverse model. Thus an expression between the output of corrector and the voltage of the inductor should be found. Thus, the following expression is proposed:

$$\alpha(s) = \frac{V_L^{'}(s) + V_{out}(s)}{\frac{4n\sqrt{2}}{\pi}\alpha(s) \times V_{in}(s)} \tag{51}$$

Where, V_L' is a new control variable represents the voltage reference of the inductor.

Thus, a linear transfer between $V_L'(s)$ and $I_L(s)$ is obtained by:

$$T_1(s) = \frac{I_L(s)}{V_L^{'}(s)} = \frac{1}{Ls} \tag{52}$$

The bandwidth of the current loop ω_i should be ten times lower than the switching frequency.

$$f_i \le \frac{f}{10}, \omega_i \le \frac{2\pi f}{10} \tag{53}$$

The inductor current loop is shown in Fig. 15.

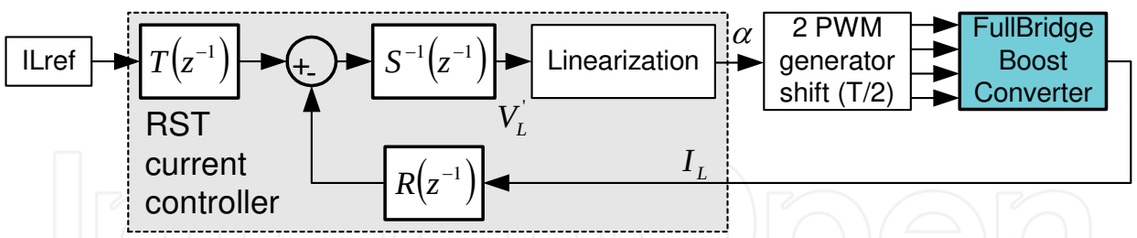

Fig. 15. Full-bridge converter inductor current control loop.

The output voltage loop was designed following a similar strategy to the current loop. To define the voltage controller, it is assumed that the current control loop is perfect. The capacitor current and voltage models are obtained by expressions 54 and 55:

$$I_C(s) = I_L(s) - I_{out}(s) \tag{54}$$

$$V_C(s) = \frac{1}{Cs}\left(I_L(s) - I_{out}(s)\right) \tag{55}$$

The linearization of the system is done by the following expression:

$$I_L(s) = I_C^{'}(s) + I_{out}(s) \Rightarrow I_{Lref}(s) = I_C^{'}(s) + I_{out}(s) \tag{56}$$

Where I'_c is a new control variable represents the current reference of the capacitor.
Thus, a linear transfer between $V_{out}(s)$ and $I'_c(s)$ is obtained by:

$$T_2(s) = \frac{V_{out}(s)}{I_C^{'}(s)} = \frac{1}{Cs} \tag{57}$$

The bandwidth of the voltage loop ω_v should be ten times lower than the current loop bandwidth ω_i which means hundred times lower than the switching frequency.

$$f_v \le \frac{f}{100}, \omega_v \le \frac{2\pi f}{100} \tag{58}$$

The output voltage control loop is shown in Fig. 16.

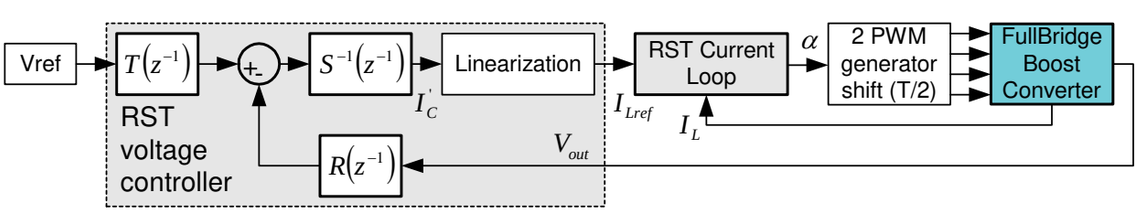

Fig. 16. Full-bridge converter output voltage control loop.

Simulation results

The efficiency of the Full-bridge dc/dc converter is about 91.5% at full load as shown in Fig. 17. The efficiency of this converter can be increased by using phase shifted PWM control and zero voltage switching ZVS technique.

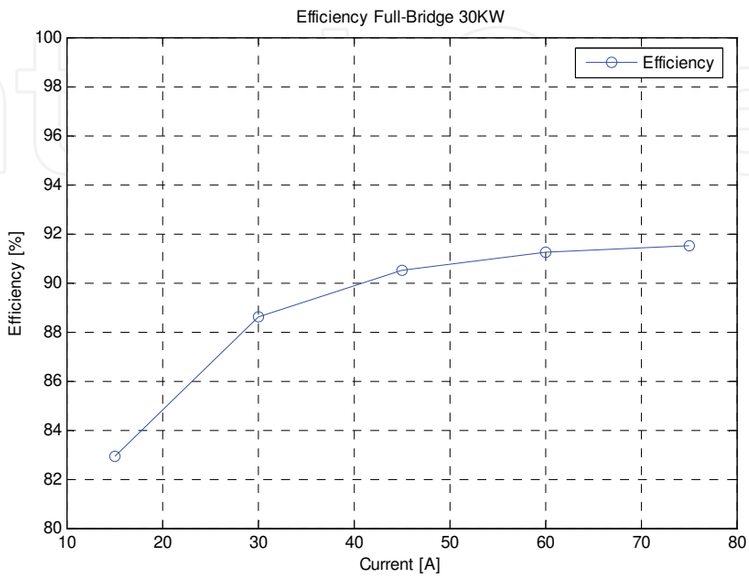

Fig. 17. Full-bridge converter efficiency versus current load.

Fig. 18 shows the spectrum of the EMI of the Full-Bridge converter. The level of conducted interference is not tolerable by the regulations. As a consequence EMI filter suppression is necessary to meet the terms the regulations.

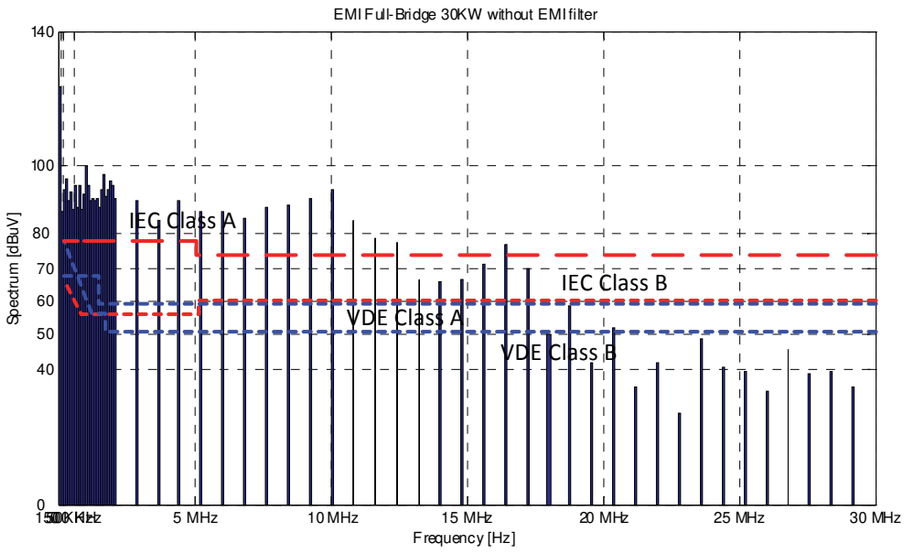

Fig. 18. EMI simulation results of Full-Bridge DC/DC converter.

7. Interpreting and comparing results

Table 4 recapitulates the volume, weight, efficiency and the EMI of each converter. The inductor volume and weight were approximated. It can be noticed that the full-bridge converter has the biggest volume and weight due to the output inductance. This inductance value can be reduced by increasing the switching frequency of the converter. We can notice that the best candidate for the application is the Interleaving multi-channel topology which has the higher efficiency and lower weight and volume. Weight and volume estimation takes into account only the IGBT, DIODE, Inductor and capacitor (transformer for full bridge) and it doesn't take into account the cooling system and the arrangement of components in the casing of the converter.

DC/DC converter	EMI	Volume(cm3)	Weight(g)	Efficiency at full load
Boost	-+	2167	6325	83%
Interleaved 4-channels	+	1380	3900	92%
Full-Bridge	--	3033	9268	91.5%

Table 4. Recapitulative table.

Fig. 19 gives an idea about the difference in the weight, volume and efficiency of each converter.

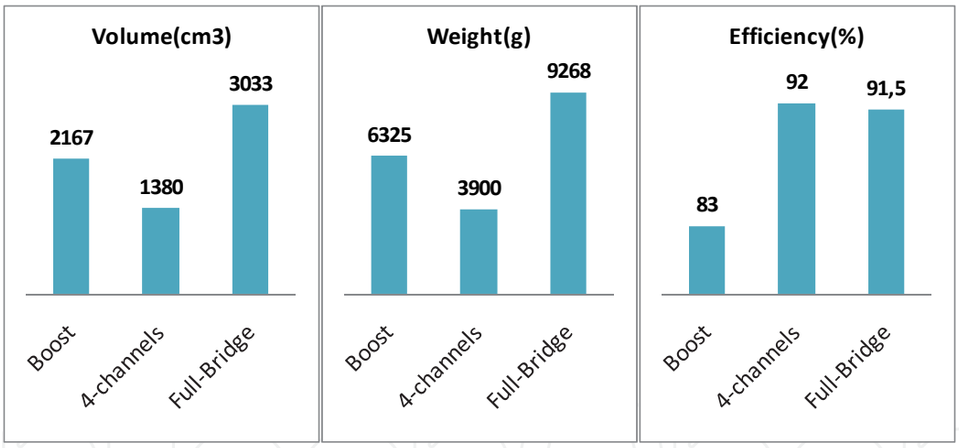

Fig. 19. Efficiency and approximated weight and volume of each converter

8. Conclusion

In this chapter, a comparative study which presents three examples of DC-DC converter topologies (Boost DC/DC converter, interleaved step-up DC/DC converter and Full-bridge step-up DC/DC converter) is carried out. The first structure considers a basic, single step-up converter; the second is based on basic interleaving technique. This structure, even simple, improves the step-up converter quality of the current drawn from the fuel cell and has small weight and volume. However, it presents limits when a high voltage step-up is required. The third topology is the full-bridge converter which has the possibility to high voltage step-up thanks to the High frequency transformer. Simulations are carried out for a three converters of 30 KW. Simulations take into account real components (IGBT and Diode), the

weight and volume of each converter were calculated based on datasheets. The efficiency of each converter was calculated for the worst case condition (maximum losses in the power switches). Simulations results show interleaved 4-channels DC/DC converter as a best candidate to the application. It has low EMI, the higher efficiency, the smaller volume and weight which are required for transport application.

9. References

Bouhalli, N., Cousineau, M., Sarraute, E., & Meynard, T. (2008). Multiphase coupled converter models dedicated to transient response and output voltage regulation studies, *Proceedings of EPE-PEMC 2008 13th Conference on Power Electronics & Motion Control*, pp. 281 - 287, ISBN 978-1-4244-1741-4, Poznan, Poland, September 1-3, 2008

Büchi, F., Delfino, A., Dietrich, P., Freunberger, S.A., Kötz, R., Laurent, D., Magne, P.A., Olsommer, D., Paganelli, G., Tsukada, A., Varenne, P. & Walser, D. (2006). Electrical Drivetrain Concept with Fuel Cell System and Supercapacitor – Results of the «HY-LIGHT» - vehicle, *VDI Tagung Innovative Fahrzeugantriebe 2006*, pp. 415-429, Dresden, Germany, 2006

Cacciato, M., Caricchi, F., Giuhlii, F. & Santini, E. (2004). A Critical Evaluation and Design of Bi-directional DC/DC Converters for Super-Capacitors Interfacing in Fuel Cell Applications, *Proceedings of IAS 39th IEEE Industry Applications Conference Annual Meeting*, pp. 1127–1133, ISBN 0-7803-8486-5, Rome, Italy, October 3-7, 2004

Chiu, H.J., & Lin, L.W. (2006). A Bidirectional DC–DC Converter for Fuel Cell Electric Vehicle Driving System, *in Power Electronics IEEE Transactions*, Vol.21 Issue 4, (2006), pp. 950–958, ISSN 0885-8993

Destraz, B., Louvrier, Y., & Rufer, A. (2006). High Efficient Interleaved Multi-channel dc/dc Converter Dedicated to Mobile Applications, *Proceedings of IAS 41st IEEE Industry Applications Conference Annual Meeting*, pp. 2518–2523, ISBN 1-4244-0364-2, Tampa, Florida, USA, October 8-12, 2006

Farhadi A., Jalilian A. (2006). Modeling and Simulation of Electromagnetic Conducted Emission Due to Power Electronics Converters, *Proceedings of PEDES'06 International Conference on Power Electronics, Drives & Energy Systems*, pp. 1-6, ISBN 0-7803-9772-X, New Delhi, India, December 12-15, 2006

Fengyan, W., Jianping, X., & Bin, W. (2006). Comparison Study of Switching DC-DC Converter Control Techniques, *Proceedings of International Conference on Communications, Circuits & Systems*, pp. 2713-2717, ISBN 0-7803-9584-0, Guilin, Alberta, Canada, June 25-28, 2006

Garcia Arregui, m. (2007). Theoretical study of a power generation unit based on the hybridization of a fuel cell stack and ultracapacitors, *Laboratoire Plasma et Conversion d'Energie*, Toulouse, France, 2007

Garcia, O., Flores, L.A., Oliver, J.A., Cobos, J.A., & De la Pena, J. (2005). Bi-Directional DC/DC Converter For Hybrid Vehicles, *Proceedings of PESC'05 IEEE 36th Power Electronics Specialists Conference*, pp. 1881–1886, ISBN 0-7803-9033-4, Recife, Brazil, June, 2005

Lachaize, J. (2004). Etude des stratégies et des structures de commande pour le pilotage des systèmes énergétiques à Pile à Combustible (PAC) destinés à la traction, *Laboratoire d'Electrotechnique et d'Electronique Industrielle de l'ENSEEIHT*, Toulouse, France, 2004

Lachichi, A., Schofield, N. (2006). Comparison of DC-DC Converter Interfaces for Fuel Cells in Electric Vehicle Applications, *Proceedings of VPPC'06 IEEE Conference on Vehicle Power & Propulsion*, pp. 1-6, ISBN 1-4244-0158-5, Windsor, UK, September 6-8, 2006

Landau, I. D. (1998). The R-S-T digital controller design and applications, *Journal of Control Engineering Practice*, Vol.6, Issue 2, (February 1998), pp. 155-165

Pepa, E. (2004). Adaptive Control of a Step-Up Full-Bridge DC-DC Converter for Variable Low Input Voltage Applications, *Faculty of the Virginia Polytechnic Institute and State University*, Blacksburg, Virginia, 2004

Schaltz, E., & Rasmussen, P.O. (2008). Design and Comparison of Power Systems for a Fuel Cell Hybrid Electric Vehicle, *Proceedings of IAS'08 IEEE Industry Applications Society Annual Meeting*, pp. 1-8, ISBN 978-1-4244-2278-4, Edmonton, Alberta, Canada, October 5-9, 2008

Yu, W., & Lai, J.S. (2008). Ultra High Efficiency Bidirectional DC-DC Converter With Multi-Frequency Pulse Width Modulation, *Proceedings of APEC 2008 23rd Annual IEEE Conference and Exposition on Applied Power Electronics*, pp. 1079-1084, ISBN 978-1-4244-1873-2 Austin, Texas, USA, February 24-28, 2008

Yu, X., Starke, M.R., Tolbert, L.M, & Ozpineci, B. (2007). Fuel cell power conditioning for electric power applications: a summary, *Journal of IET electric power applications*, Vol.1, No.5, (2007), pp. 643-656, ISSN 1751-8660

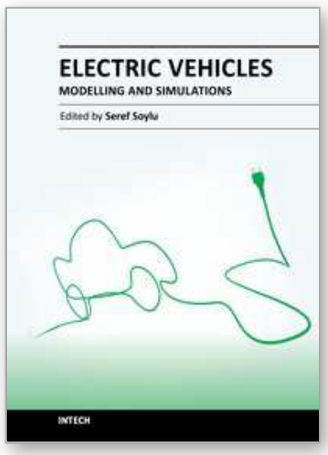

Electric Vehicles - Modelling and Simulations

Edited by Dr. Seref Soylu

ISBN 978-953-307-477-1
Hard cover, 466 pages
Publisher InTech
Published online 12, September, 2011
Published in print edition September, 2011

In this book, modeling and simulation of electric vehicles and their components have been emphasized chapter by chapter with valuable contribution of many researchers who work on both technical and regulatory sides of the field. Mathematical models for electrical vehicles and their components were introduced and merged together to make this book a guide for industry, academia and policy makers.

InTech Europe
University Campus STeP Ri
Slavka Krautzeka 83/A
51000 Rijeka, Croatia
Phone: +385 (51) 770 447
Fax: +385 (51) 686 166
www.intechopen.com

InTech China
Unit 405, Office Block, Hotel Equatorial Shanghai
No.65, Yan An Road (West), Shanghai, 200040, China
中国上海市延安西路65号上海国际贵都大饭店办公楼405单元
Phone: +86-21-62489820
Fax: +86-21-62489821

IntechOpen